Imaging subsurface damage of grinded fused silica optics by confocal fluorescence microscopy

Jérôme Neauport, P Cormont, P Legros, C Ambard, J Destribats

Imaging subsurface damage of grinded fused silica optics by confocal fluorescence microscopy

J. Neauport,[1*] P. Cormont,[1] P. Legros,[2] C. Ambard,[3] J. Destribats[1]

[1] *Commissariat à l'énergie atomique, Centre d'études scientifiques et techniques d'Aquitaine, BP 2, 33114 Le Barp, France*

[2] *Plate-forme d'Imagerie Cellulaire de l'Institut des Neurosciences, Institut François Magendie, 146 rue Léo-Saignat, Université de Bordeaux II, France*

[3] *Commissariat à l'énergie atomique, Centre du Ripault, BP 16, 37260 Monts, France*

**Corresponding author: jerome.neauport@cea.fr*

Abstract: We report an experimental investigation of fluorescence confocal microscopy as a tool to measure subsurface damage on grinded fused silica optics. Confocal fluorescence microscopy was performed with an excitation at the wavelength of 405 nm on fixed abrasive diamond grinded fused silica samples. We detail the measured fluorescence spectrums and compare them to those of oil based coolants and grinding slurries. We evidence that oil based coolant used in diamond grinding induces a fluorescence that marks the subsurface damages and eases its observation. Such residual traces might also be involved in the laser damage process.

OCIS codes: (140.3330) Lasers and laser optics: laser damage; (220.5450) Optical design and fabrication: polishing; (110.0180) Imaging systems: microscopy; (160.0160) Materials: fluorescent and luminescent materials.

References and links

1. M. L. André, "Status of the LMJ project," in Solid state lasers for application to Inertial Confinement Fusion: Second Annual International Conference, M. L. André, ed., Proc. SPIE **3047**, 38-42 (1996).
2. W. H. Lowdermilk, "Status of the National Ignition Facility project," in Solid state lasers for application to Inertial Confinement Fusion: Second Annual International Conference, M. L. André, ed., Proc. SPIE **3047**, 16-37 (1996).
3. S. G. Demos, M. Staggs, and M. R. Kozlowski, "Investigation of Processes Leading to Damage Growth in Optical Materials for Large-Aperture Lasers," Appl. Opt. **41,** 3628-3633 (2002).
4. H. Bercegol, P. Bouchut, L. Lamaignere, B. Le Garrec, and G. Raze, "The impact of laser damage on the lifetime of optical components in fusion lasers," in *Proceedings of Laser-induced Damage Threshold in Optical Materials : 2003,* G. J. Exarhos, A. H. Guenther, N. Kaiser, K. L. Lewis, M. J. Soileau, C. J. Stolz, Eds, Proc. SPIE **5273**, 312-324 (2004).
5. D. W. Camp et al., "Subsurface damage and polishing compound affect the 355 nm laser damage threshold of fused silica surfaces," in *Proceedings of Laser-induced Damage Threshold in Optical Materials,* Proc. SPIE **3244**, 356-364 (1998).
6. S. Papernov and A. W. Schmid, "Correlations between embedded single gold nanoparticles in SiO2 thin film and nanoscale crater formation induced by pulse-laser radiation," J. Appl. Phys. **92**, 5720-5728 (2002).
7. F. Bonneau, P. Combis, J. L. Rullier, J. Vierne, H. Ward, M. Pellin, M. Savina, M. Broyer, E. Cottancin, J. Tuaillon, M. Pellarin, L. Gallais, J. Y. Natoli, M. Perra, H. Bercegol, L. Lamaignere, M. Loiseau, and J. T. Donohue "Study of UV laser interaction with gold nanoparticles embedded in silica," J. Appl. Phys. B **75**, 803-815 (2002).
8. J. Neauport, L. Lamaignere, H. Bercegol, F. Pilon, and J-C Birolleau, "Polishing-induced contamination of fused silica optics and laser induced damage density at 351 nm," Opt. Express **13**, 10163-10171 (2005).
9. F. Y. Genin, A. Salleo, T. V. Pistor, and L. L. Chase, "Role of light intensification by cracks in optical breakdown on surfaces," in J. Opt. Soc. Am. A **18** 10, 2607-2616 (2001).
10. M. D. Feit and A. M. Rubenchik, "Influence of subsurface cracks on laser induced surface damage," in *Proceedings of Laser-induced Damage Threshold in Optical Materials : 2003,* G. J. Exarhos, A. H. Guenther, N. Kaiser, K. L. Lewis, M. J. Soileau, and C. J. Stolz, Eds, Proc. SPIE **5273,** 264-272 (2004).
11. A. Salleo, F. Y. Genin, J. M. Yoshiyama, C. J. Stolz, and M. R. Kozlowski, "Laser-induced damage of fused silica at 355 nm initiated at scratches," in *Proceedings of Laser-Induced Damage in Optical Materials: 1997,* Gregory J. Exarhos, Arthur H. Guenther, Mark R. Kozlowski, and M. J. Soileau, Eds, Proc. SPIE **3244,** 341-347 (1998).

#105390 - $15.00 USD Received 15 Dec 2008; revised 20 Jan 2009; accepted 21 Jan 2009; published 23 Feb 2009

12. J. Neauport, P. Cormont, C. Ambard, and F. Pilon, "Concerning the impact of polishing induced contamination of fused silica optics on the laser-induced damage density at 351 nm," Optics Comm. **281** 3802–3805 (2008).
13. H. Bercegol, P. Grua, D. Hébert, and J. P. Morreeuw, "Progress in the understanding of fracture related damage of fused silica," in *Proceedings of Laser-Induced Damage in Optical Materials: 2007,* Gregory J. Exarhos, Arthur H. Guenther, Keith L. Lewis, Detlev Ristau, M. J. Soileau, and C. J. Stolz, Eds, Proc. SPIE **6720,** 1-12 (2007).
14. W. J. Rupp, "Mechanism of the diamond lapping process," Appl. Opt. **13**, 6, 1264-1269.
15. P. Hed and D. F. Edwards, "Optical glass fabrication technology. 2: Relationship between surface roughness and subsurface damage," Appl. Opt. **26**, 4677-4680 (1987).
16. J. C. Randi, J. C. Lambropoulos, and S. D. Jacobs, "Subsurface damge in some single crystalline optical materials," Appl. Opt. **44** 12, 2241-2249 (2005).
17. T. Suratwala, L. Wong, P. Miller, M. D. Feit, J. Menapace, R. Steele, P. Davis, and D. Walmer, " Sub-surface mechanical damage distributions during grinding of fused silica," J. Non Cryst. Sol. **352,** 5601-5617 (2006).
18. Z. Wang, Y. Wu, Y. Dai, and S. Li, "Subsurface damage distribution in the lapping process," Appl. Opt. **47** 10, 1417-1426 (2008).
19. Y. Zhou, P. D. Funkenbusch, D. J. Quesnel, D. Golini, and A. Lindquist, "Effect of etching and imaging mode on the measurement of subsurface damage in microground optical glasses," J. Am. Ceram. Soc. **77**, 3277-3280 (1994).
20. O. Fahnle, T. Wons, T. Koch, E. Debruyne, S Meeder, M. Booij, and S. M. Braat, "iTIRM as a tool for qualifying polishing processes," Appl. Opt. **41**, 4036-4038 (2002)
21. A. Wuttig, J. Steinert, A. Duparre, and H. Truckenbrodt, "Surface roughness and subsurface damage charaacterization of fused silica substrates," in Proceedings of the *EUROPTO conference on topical fabrication and testing*, Proc. SPIE **3739**, 369-376 (1999).
22. L. Nevot and P. Croce, "Sur l'étude des couches superficielles monoatomiques par reflexion rasante (spéculaire ou diffuse) de rayons X par la méthode de l'empilement sandwich," J. Appl. Cryst. **8**, 304-314 (1975).
23. LEICA TCS SP2 confocal microscope, http://www.leica-microsystems.com/products/tcs-sp2_key .
24. J. A. Menapace, P. J. Davis, W. A. Steel, T. I. Suratwala, P. E. Miller, and L. L. Wong, "Utilization of magnetorheological finishing as a diagnostic tool for investigating 3D structure of fractures in fused silica," in *Proceedings of Laser-Induced Damage in Optical Materials: 2005,* Gregory J. Exarhos, Arthur H. Guenther, Keith L. Lewis, Detlev Ristau, M. J. Soileau, Christopher J. Stolz, Eds, Proc. SPIE **5991**, 201-213 (2005).
25. S. G. Demos, M. Staggs, K. Minoshima, and J. Fujimoto, "Characterization of laser induced damage sites in optical components", Opt. Express **10**, 1444-1450 (2005).
26. Mark R. Kozlowski, and Stavros G. Demos "Properties of modified silica detected within laser-induced damage sites," in Proceeding of Inorganic Optical Materials II 2000, Alexander J. Marker III, Eugene G. Arthurs, Eds, Proc. SPIE **4102** 106-111 (2000).
27. S. O. Kucheyev and S. G. Demos, "Optical defects produced in fused silica during laser-induced breakdown," App. Phys. Let. Vol **82**, 3230-3232 (2003).
28. P. Barritault, P. Bouchut, H. Bercegol, P. Chaton, and G. Ravel, "Fluorescence of mitigated laser damages in fused silica," Laser-Induced Damage Opt. Materials: 2004, edited by G. J. Exarhos, A. H. Guenther, N. Kaiser, K. L. Lewis, M. J. Soileau, and C. J. Stolz Eds, Proceedings of SPIE Vol. **5647**, 188-196 (2005).

1. Introduction

Fusion class power laser facilities such as Megajoule laser (LMJ) [1] or National Ignition Facility (NIF) [2] will focus between 1.5 and 1.8 MJ of energy at the wavelength of 0.351 µm, in the center of an experiment chamber. After amplification and transport at the wavelength of 1.053 µm, frequency conversion at 0.351 µm is done with two KH_2PO_4 crystals. Afterward, optics used to convey, focus or shape the laser beam are large fused silica optics working in transmission. When exposed to fluences of some joules per centimeter square at the wavelength of 0.351 µm with nanosecond pulse duration, fused silica optics can exhibit localized damage. Damage sites grow exponentially after further laser exposition [3] and therefore dramatically limit the optic lifetime. Hence, understanding laser damage initiation and growth of fused silica optics at the wavelength 0.351 µm has been subject to major efforts in the last decade. Since optics operational durability is governed both by damage initiation and damage growth [4], strategies were developed to inhibit damage growth using CO_2 laser annealing and efforts were made to reduce damage initiation. Early works have shown that damage can initiate on local absorption of polishing process induced contaminants embedded into the fused silica optics interface [5-8] or on mechanical subsurface damage (SSD) [5, 9,

#105390 - $15.00 USD Received 15 Dec 2008; revised 20 Jan 2009; accepted 21 Jan 2009; published 23 Feb 2009

10] or surface damage [11]. Moreover, it was recently shown that for low process contaminant level samples, damage density becomes independent of the contaminant level [12]. Consequently, SSD is more likely to be the principal cause of damage. This is moreover assessed by a recent physic model explaining how damage can initiate onto a subsurface fracture [13].

SSD consists in micro cracks created by the action of hard abrasive grains involved in the material removal process onto the brittle surface of fused silica during cutting, diamond grinding or loose abrasive grinding. Generated cracks can extend from microns to hundred microns below the surface [14-17] depending on the abrasive type and manufacturing conditions (pressure, plate hardness, speed …) [18]. After final polishing, most of the SSD is removed but some residual cracks might still be embedded under the polishing i.e. Beilby layer.

Considering the major role of SSD in laser damage at the wavelength of 0.351 µm, efforts have been made to limit its extension during the manufacturing process and consequently to be able to measure SSD at each step of the polishing process from sawing to final polishing [14-18]. Most of the SSD measurement methods are destructives ones. Ball dimpling [19], taper method [15], magneto rheological (MRF) dimpling [16] or MRF taper polishing [17] consist in exposing the SSD of the surface to be characterized by a supposed non invasive polishing process. After an acid etching to open cracks, optical microscopy can be carried out to measure the SSD depth knowing the amount of material removed by the latter polishing process. Based on these methods, an empirical relation linking SSD depth with surface roughness p-v (R_z) was assessed: SSD = k. R_z, where k is a constant. k factor can range from 1.4 to 9.1 depending on the author, but Suratwala [17] demonstrated thanks to large area MRF taper polishing SSD measurements that the latter factor was closer to reality for fused silica large laser optics.

Non destructive measurement techniques were also studied such as total internal reflection microscopy (iTIRM) [20], white light interferometry [21] or X ray scattering [22] but they appeared to be less sensitive than destructive methods. We herein study the possibilities of confocal microscopy with or without fluorescence imaging as a tool to characterize SSD of diamond grinded samples. Manufacturing of the samples is detailed in section 2. Section 3 is devoted to the description of confocal microscopy; surface roughness measurement is also explained. Results are finally presented and discussed in section 4; we demonstrate that SSD measured depths by our methods are in good concordance with results from the literature.

2. Sample preparation methods

Fused silica samples were manufactured using various grinding or lapping processes. Samples were made using a Heraeus HOQ fused silica blank. Sample preparation methods are given in Table 1.

Table 1. Sample preparation methods

S/N	Size (diameter, thickness)	Process type	Last abrasive or diamond tool used	Mean Surface roughness R_a (µm)	Surface roughness p-v R_z (µm)
D1	50 mm / 3.5 mm	Diamond grinding	D181	1.22 ± 0.24	16.86 ± 4.34
D2	100 mm / 9 mm	Diamond grinding	D181	1.22 ± 0.14	10.94 ± 2.16
D3	100 mm / 9 mm	Diamond grinding	D64	0.13 ± 0.01	2.34 ± 0.44
D4	100 mm / 9 mm	Diamond grinding	D20	0.04 ± 0.01	0.82 ± 0.19

Samples D2, D3 and D4 were machined on a SCHNEIDER SLG 100 grinder. Parts were first processed with a D181 metallic bound diamond wheel. Samples D3 and D4 had an extra D64 resinoid bound processing. Material removal was sufficient to ensure that the residual

#105390 - $15.00 USD Received 15 Dec 2008; revised 20 Jan 2009; accepted 21 Jan 2009; published 23 Feb 2009

SSD was coming from the last grinding step based on an evaluation using Suratwala relation [17]. Sample D4 had an extra D20 resinoid bound processing compared to D64 with sufficient material removal to ensure that SSD was coming from this last processing step.

In the case of sample D1, we wanted to observe SSD from the back side of the sample. Hence thin parts of some hundred microns were necessary. Since diamond grinding of such thin part is difficult, we decided to glue together two polished samples of 3 mm thickness with index matching glue (see Fig. 1). One side of sample D1 was then machined on a SCHNEIDER SLG 100 grinder. Part was processed with a D181 metallic bound diamond wheel. Final thickness of the part was about 4 mm. Parts were then unglued. The machined side of the sample was finally glued on another sample to ensure a good stiffness and allow its observation from the backside.

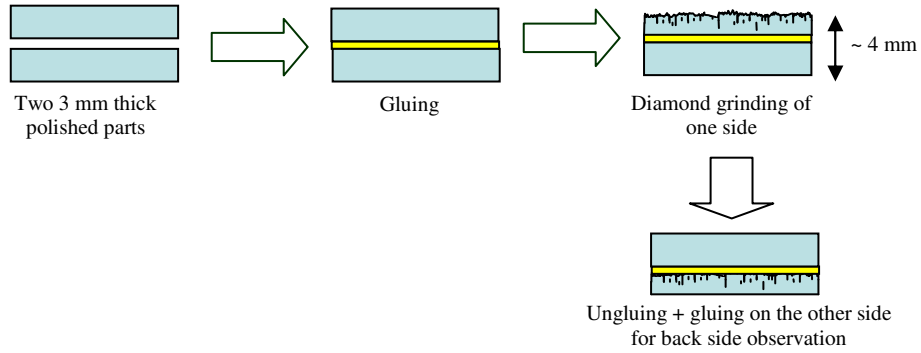

Fig. 1. Sample preparation method of sample D1

The mean surface roughness R_a and surface roughness pic-to-valley R_z of grinded or lapped sides of all the samples were then measured using a PHYNIX TR200 stylus profilometer. Values are obtained with 16 measurements equally placed radially on each sample surface with a scanning length of 4 mm. Incertitude is given at one standard deviation.

Rough surfaces such as D181 or D64 grinded surfaces are sometimes difficult to image on a confocal microscopes. The important amount of diffusion coming from the interface tends to blur the subsurface images. We therefore imagined strategies to overcome this difficulty; they are summarized in table 2.

Table 2: Sample preparation to ease confocal microscopy observation

S/N	Process type	Type of surface preparation to ease confocal measurement
D1	Diamond grinding	Backside observation after back side etching
D2	Diamond grinding	Observation in a MRF dimple
D3	Diamond grinding	Observation in a MRF dimple
D4	Diamond grinding	Observation in a MRF dimple

Samples D2, D3 and D4 were processed on one side with a MRF QED Q22 polishing machine to make a dimple similar to those made for MRF dimpling [16]. Confocal microscopy could then be made on one side in the MRF dimple. For sample D1, after the part preparation previously described, the back polished side of the sample was thinned down with an HF/HNO3 solution. Part D1 thickness after etching was about 550 to 600 µm. Confocal observation then was carried out from the back polished and etched surface.

3. Sample characterization methods

Manufactured samples were measured using a confocal microscope. A confocal microscope is an integrated microscope system consisting of a fluorescence microscope, laser light sources,

#105390 - $15.00 USD Received 15 Dec 2008; revised 20 Jan 2009; accepted 21 Jan 2009; published 23 Feb 2009

a scan head which directed the laser on the sample and collected the emission, a computer with software for controlling the scan head and display the acquisition. Confocal microscope can be used in several modes, epi-fluorescence laser scanning mode (ELSM), reflectivity mode and transmitted mode. We will focus on the two first ones that were used for the study. As shown in Fig. 3, excitation in ELSM which comes from laser point source arrives confocally on the fluorescent sample. Fluorescent light emitted from the point illuminated is focused as a confocal point at the detector pinhole. Fluorescent light emitted from the out of focus point (above and below the focus plane) doesn't enter the pinhole and thus is not detected. By scanning the sample in x and y direction we can reconstruct an image. To achieve a 3D reconstruction the x, y stage is motorised in z direction. For the separation of excitation and emitted light a dichroic mirror is used and a filter is placed in front of the detector (Photomultiplier). In reflectivity laser scanning mode we are not taking back the fluorescence of the sample but the reflection of the laser on the sample. For this purpose, the dichroic mirror is exchange with a semi reflective mirror to get the reflected light on the photomultiplier. The reflected light comes as well through the pinhole to achieve a confocal resolution.

Resolution $\sigma_{x,y}$ in x and y directions and σ_z in z direction in confocal microscopy are given by the following formula $\sigma_{x,y} = 0.4\ \lambda / NA$ and $\sigma_z = 1.4\ \lambda n / NA^2$, where NA is the numerical aperture, λ is the wavelength and n the optical index. Typical resolutions of approximately 150 nm in x-y and 300 nm in z are reached with the 40x and 63x objectives used.

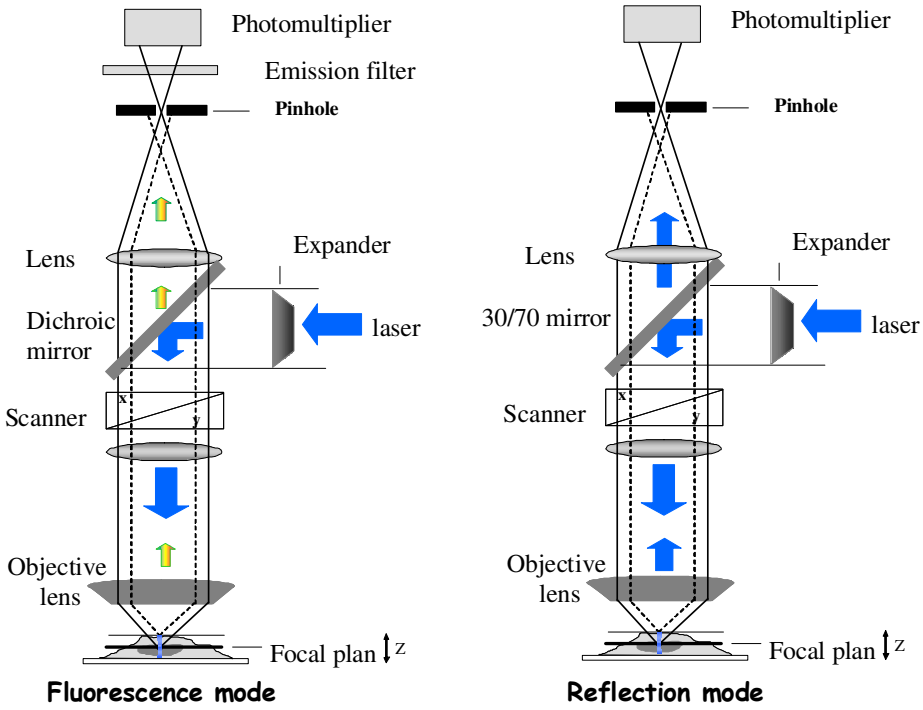

Fig. 3. Confocal microscopy principle: epifluorescence mode (left) and reflection mode (right)

Measurements were done using a Leica DMR upright TCS SP2 AOBS [23] equipped with a 405 nm laser diode and a 458 nm Argon laser. On this confocal microscope, an AOBS (acousto optic beam splitter) crystal is used instead of a dichroic mirror. It allows a simultaneous measurement of both fluorescence and reflectivity images. Instead of using normal filter for selecting the wavelength, the leica confocal uses a prism system. After the pinhole a prism is introduced along the beam way, to spread spatially the wavelengths, a slit

#105390 - $15.00 USD Received 15 Dec 2008; revised 20 Jan 2009; accepted 21 Jan 2009; published 23 Feb 2009

system then collects the fluorescence to the desired wavelengths. With this system, bandwidth from 5 nm till 300 nm can be selected.

All images were made using the 405 nm laser diode (fluorescence mode) or the 458 nm Argon laser (reflection mode), a 63 x objective with NA of 1.4 or a 40 x objective with NA of 1.25. 3D reconstitution and image analysis was performed with Imaris software v 6.0 from Biplane Company. Images were made with a scan speed of 400 lines/second; pinhole is 1 airy; spectral reception is between 435 to 661 nm. For the spectral acquisition we use as often as possible a window of 5 nm (regarding to the amount of fluorescence available), the sampling step is 2.5 nm, and pinhole is rather large (>2 airy) to ensure maximal signal captaincy.

4. Results and discussions

4.1 Samples D1 and D2 – D181 diamond grinding

Measurement results of sample D2 are given below. Images show the surface of the sample inside the MRF dimple in reflection at 458 nm (top left) and in fluorescence mode (top right, excitation at 405 nm, 435 nm – 661 nm spectral band) on an identical area of 1.5 mm x 1.5 mm.

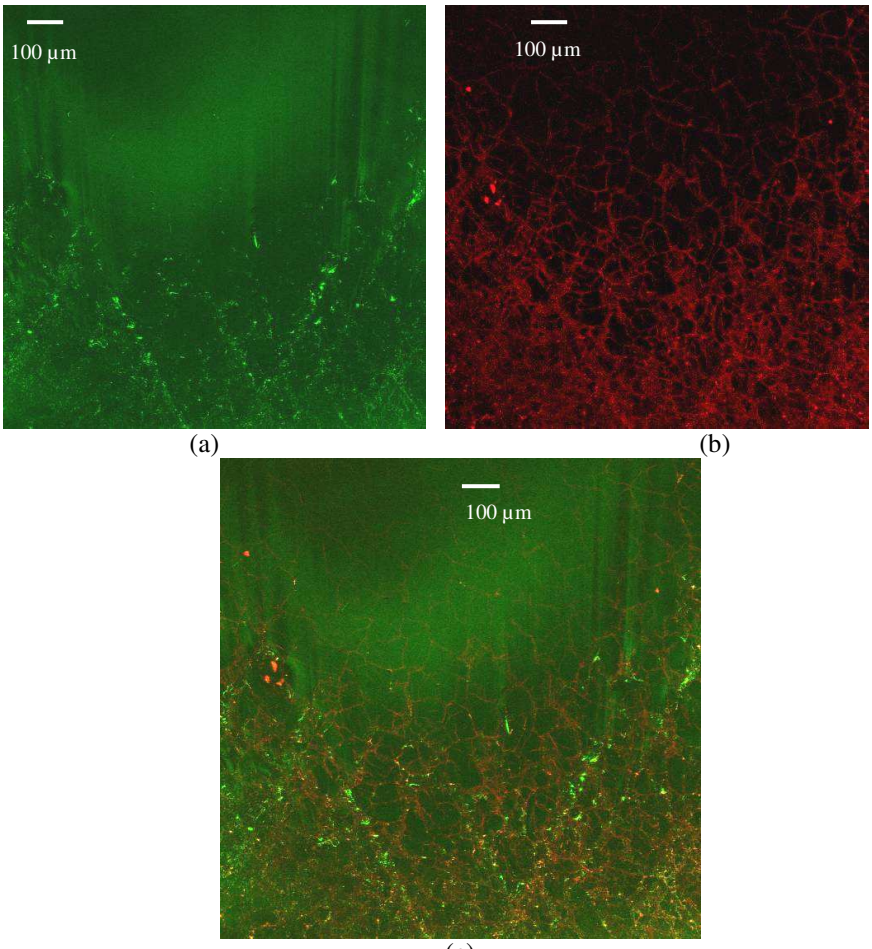

Fig. 4. Sample D2 – Confocal microscopy image of the surface in the MRF dimple on an area of 1.5x1.5 mm², approximately 50 µm removed by MRF between border of the dimple and top of the figure. Same area measured in reflection at 458 nm (a), fluorescence in the 435-661nm spectral band for an excitation wavelength of 405 nm (b) and superposition of the two images (c) – 63 x objective

#105390 - $15.00 USD Received 15 Dec 2008; revised 20 Jan 2009; accepted 21 Jan 2009; published 23 Feb 2009

Comparison of these images reveals that subsurface fractures are mainly observed on the confocal microscopy acquisition made in fluorescence mode. To demonstrate that fractures seen in fluorescence mode are subsurface ones, we etched the surface of the dimple with a HF/HNO3 (80%-20%) solution during 2 minutes. This light etch should open SSD and make it visible by standard microcopy. Figure 5 shows the result of the superposition of Fig. 4(c) and of the standard microscopy image after the light etching. It is evidenced that open cracks revealed in fluorescence mode correspond to those open by the etching and seen in standard microscopy.

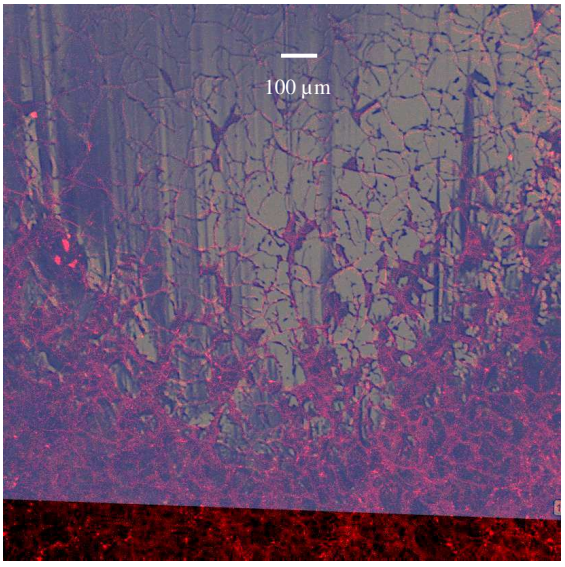

Fig. 5. Sample D2, area of 1.5 x 1.5 mm² – Standard microscopy image (in light grey) after light HF etching to reveal cracks superposed to Fig. 4(c) i.e. image in fluorescence mode before etching (red) and reflection mode (green) – 63 x objective

Confocal microscopy was also made on sample D1 with an observation carried out from the back side. Result is shown in fluorescence mode in Fig. 6 (Media 1). Total depth is 224 µm with 60 sections made and a scan area of 227 µm x 227 µm. The structure of the SSD is very similar to previous results from Menapace [24]. Moreover, SSD depth measured by confocal microscopy is approximately 190 µm, in good concordance with an evaluation from the surface roughness measurement (table 1) using Suratwala relation [17] which gives 153 ± 39 µm.

#105390 - $15.00 USD Received 15 Dec 2008; revised 20 Jan 2009; accepted 21 Jan 2009; published 23 Feb 2009

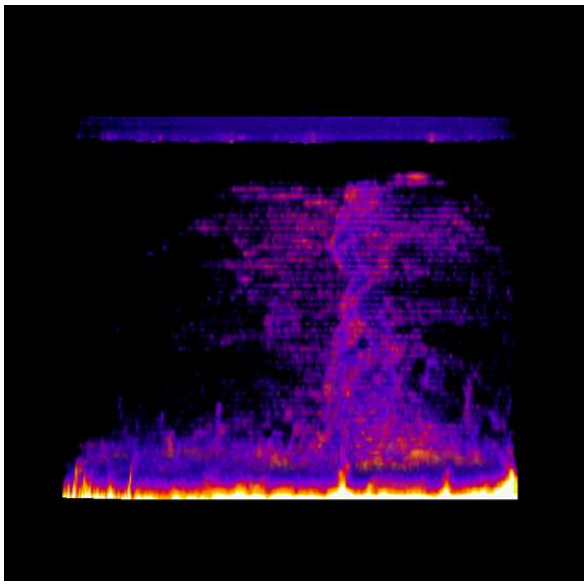

Fig. 6. Sample D1 – Confocal microscopy in fluorescence mode in the 435 nm – 661 nm band (405 nm excitation). Diamond grinded surface is at the bottom, measurement carried out from the back side i.e. top of the figure. (Media 1). 63 x objective

In order to get a better understanding of the source of the fluorescence of the SSD, we made some spectrums of subsurface fractures; results are the same on both D1 and D2 samples. Figure 7 details the obtained results on sample D1.

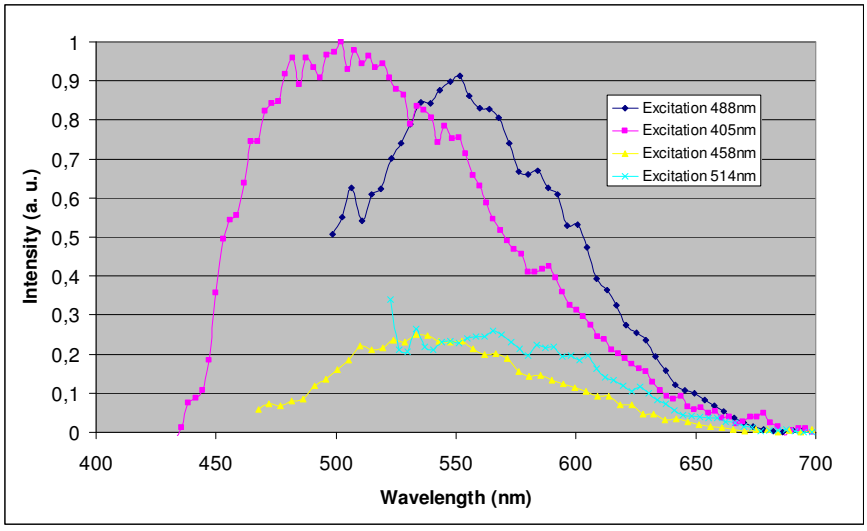

Fig. 7. Sample D1 – Fluorescence spectrum for different excitation wavelengths measured on SSD. Spectrums are normalized to 1 to be compared.

Spectrums were made with excitation wavelength of 405 nm, 456 nm, 488 nm and 514 nm. All spectrums were normalized to the maximum signal measured at 405 nm. Fluorescence is important for an excitation wavelength of 405 nm, become weak at 458 nm, increases at 488 nm and decreases at 514 nm to become null at higher wavelength.

#105390 - $15.00 USD Received 15 Dec 2008; revised 20 Jan 2009; accepted 21 Jan 2009; published 23 Feb 2009

4.2. Sample D3 – D64 diamond grinding

Results of observations carried out on sample D3, inside the MRF dimple are presented on Fig. 8 in reflection at 458 nm (in green) and in fluorescence mode (in red, 435 nm – 661 nm spectral band for an excitation of 405 nm) on an identical area of 90 µm x 90 µm. The superposition of both images demonstrates that fluorescence mode reveals subsurface fractures not seen in reflection mode. Fluorescence spectrum is identical as on sample D1 and D2.

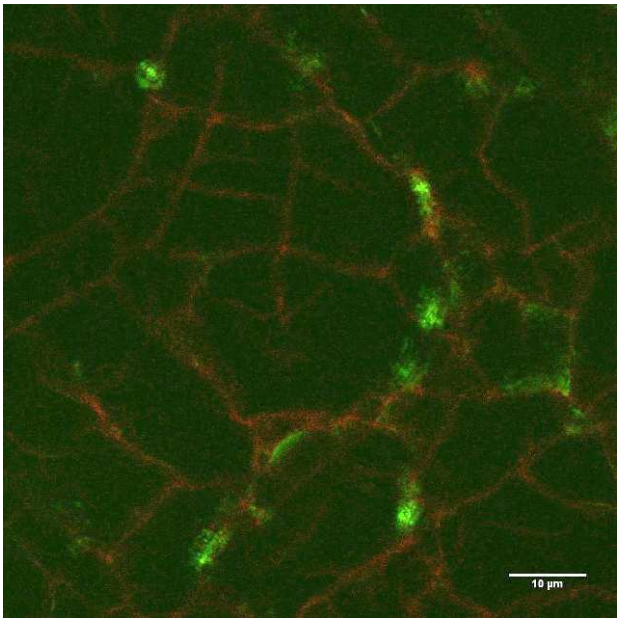

Fig. 8. Sample D3 – Confocal microscopy image of the surface in the MRF dimple on an area of 90x90 µm². Superposition of image in reflection mode at 458 nm (in green), and image in fluorescence mode in the 435-661nm spectral band for an excitation wavelength of 405 nm(in red)

A depth profile of the SSD on a small area of 20 µm x 20 µm is also presented on Fig. 9. Structure is very similar D181 machined samples D1 and D2.

#105390 - $15.00 USD Received 15 Dec 2008; revised 20 Jan 2009; accepted 21 Jan 2009; published 23 Feb 2009

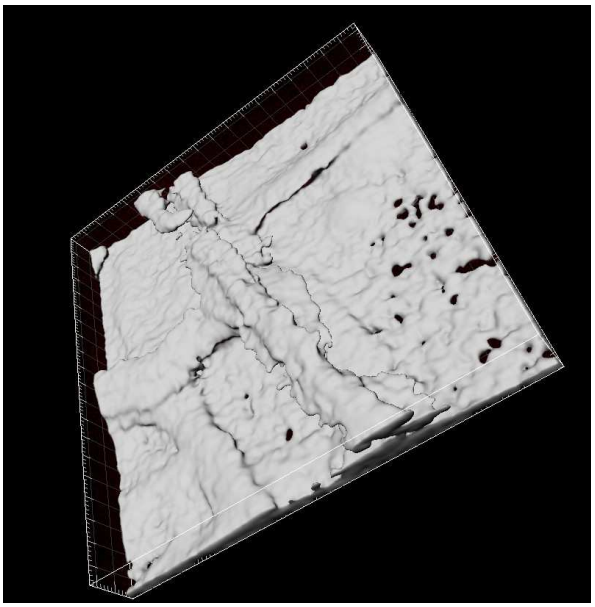

Fig. 9. Sample D3 – Confocal microscopy image in fluorescence mode (405 nm excitation wavelength) in the MRF dimple on an area of 20x20 µm². Surface rendering is done to show structure of the SSD. Dimple surface is on the back of the image.

4.3. Samples D4 – D20 diamond grinding

Results of observations inside the MRF dimple carried out on sample D4, are shown on Fig. 9. Reflection at 458 nm is represented in green; fluorescence mode (435 nm – 661 nm spectral band, 405 nm excitation wavelength) is represented in red on an identical area of 373 µm x 373 µm.

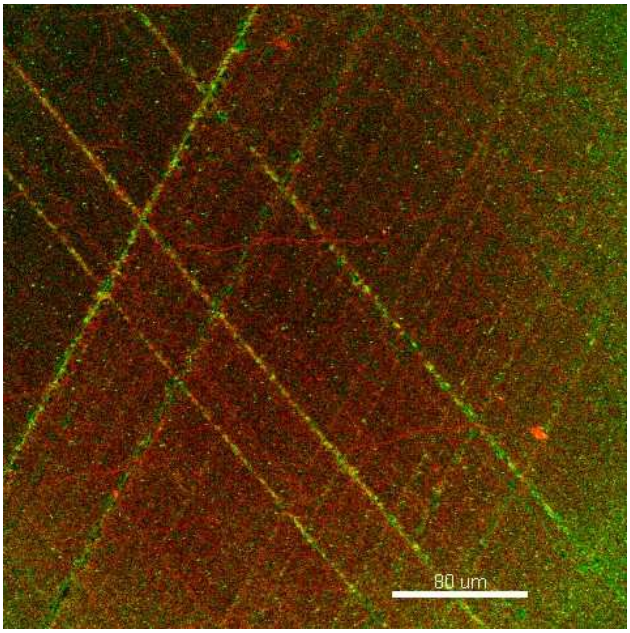

Fig. 10. Sample D4 – Confocal microscopy image of the surface in the MRF dimple on an area of 373 x 373 µm². Superposition of image in reflection mode at 458 nm (in green), and image in fluorescence mode in the 435-661nm spectral band for an excitation wavelength of 405 nm (in red) – 40x objective.

#105390 - $15.00 USD Received 15 Dec 2008; revised 20 Jan 2009; accepted 21 Jan 2009; published 23 Feb 2009

The superposition of both images demonstrates that fluorescence mode reveals on more time the subsurface fractures not seen in reflection mode. In peculiar, fine horizontal subsurface fractures can be seen on this sample. Fluorescence spectrum is identical as on sample D1 and D2.

4.4. Fluorescence potential sources

We have shown from the previous measurements that fluorescence can be seen on the SSD of diamond grinded parts. Whatever the grinding combination carried out or the type of observation (from the top or the bottom, with of without polishing), this fluorescence exists with a pick centred at 505 nm for an excitation wavelength of 405 nm. Diamond grinder usually used water soluble oil based coolants to ease the diamond wheel cutting during the process. We measured the fluorescence spectrum of a freshly prepared coolant identical to the one used on the SCHNEIDER grinder during the processing of our samples. A drop of soluble oil was placed between microscopy slides and measured on the LEICA DMR confocal microscope in the same manner than the silica samples measured herein. Results of the measurement are shown on Fig. 11 for an excitation wavelength of 405 nm and compared to the spectrum obtained on sample D1.

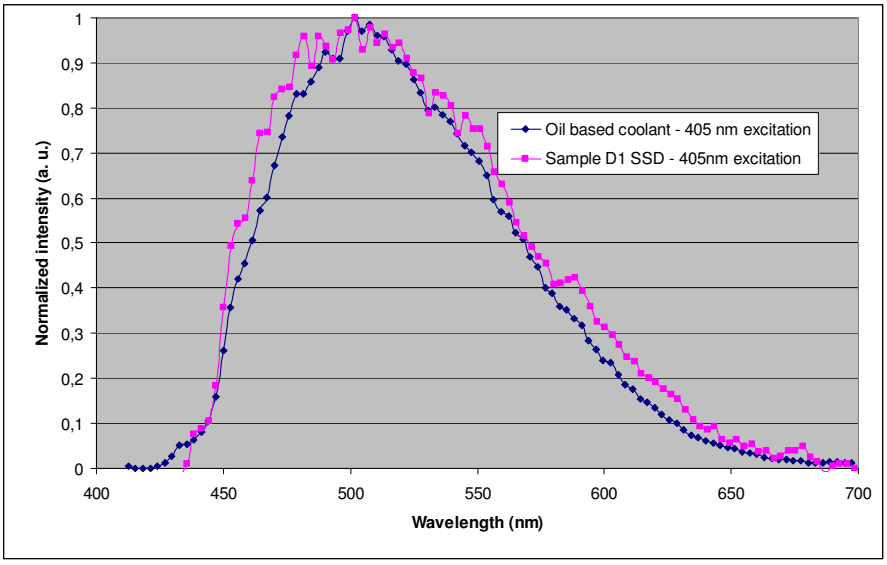

Fig. 11. Fluorescence spectrum for an excitation wavelength of 405 nm of the oil based coolant and the SSD of sample D1.

Both spectrums are identical showing that the fluorescence observed for an excitation wavelength of 405 nm on the diamond grinded samples is due to traces of coolant buried inside the SSD during the cutting process. At higher excitation wavelengths, the oil coolant exhibits no measurable fluorescence.

Consequently at higher wavelength, fluorescence of SSD shall be related to bulk fractured fused silica. The highest pic at higher wavelength is centered at 555 nm (2.23 eV) and has a half width of 100 nm (0.28eV). This pic is similar to the fluorescence centered at 2.2 eV, half width of 0.28 eV, observed by Demos on a laser damage site on fused silica with an excitation wavelength of 351 nm [25-27]. Such a behavior was also seen by Barritault on both laser damage and mitigated sites on fused silica [28]. If it has already been reported, the nature of the 555 nm peak in the emission spectrum under a 351 nm or 405 nm excitation is not clear.

Fluorescence of SSD of diamond grinded samples is then understood to be the superposition of two peaks. A first one centered at 505 nm for an excitation wavelength of 405 nm is coming from the oil coolant used during the manufacturing process. A second one, centered at 555 nm for an excitation wavelength of 488 nm is similar to what previously

#105390 - $15.00 USD Received 15 Dec 2008; revised 20 Jan 2009; accepted 21 Jan 2009; published 23 Feb 2009

observed [24-26] on laser damage sites on silica parts. Such laser damage exhibits deep cracks rather similar to subsurface cracks in SSD. The two weak emissions for excitation wavelength of 458 nm and 514 nm could be residues of the previous picks.

5. Conclusion

Plane fused silica samples were machined on a grinder with diamond wheel of decreasing granulometry from D181 down to D20. Parts exhibit different surface roughness, hence subsurface damage of various depths. Samples were prepared by two different means in order to decrease surface roughness and ease SSD observation by confocal microscopy. Confocal microscopy, carried out on a LEICA DMR SP2, reveals the existence of a fluorescence of the SSD with most intense picks at 505 nm (excitation of 405 nm) and 555 nm (excitation of 488 nm). The first pick is likely to be induced by a pollution of the SSD by the water soluble oil coolant used during grinding. The latter pick was already reported on laser damage sites on fused silica parts [25-28]. Subsurface features observed in fluorescence mode are not observed in reflection mode; hence making confocal microscopy in fluorescence mode is a powerful tool for the development of low SSD polishing processes. Even if SSD fluorescence intensity seems to decrease with tool granulometry, some tiny traces of this fluorescence might still be present in polished parts and involved in the damage process of fused silica optics at 0.351 µm. We are currently beginning some experiments to address this peculiar point on polished samples

Acknowledgments

This work is supported by the Conseil Régional d'Aquitaine and is performed in the framework of the EFESO project. We would like to acknowledge C. Luitot for its contribution to confocal microscopy on fused silica parts, C. Andre and E. Fargin for early sample preparation and measurements as well as fruitful discussions. The authors wish also to thank P. Grua, H. Bercegol and J. P. Morreeuw for interesting discussions concerning the physics of laser damage. We would like to thank SESO Company from their help in the samples preparation.

#105390 - $15.00 USD Received 15 Dec 2008; revised 20 Jan 2009; accepted 21 Jan 2009; published 23 Feb 2009